STRUCTURAL CHEMISTRY

ISSN: 2053-2296
journals.iucr.org/c

Methyl β-lactoside [methyl β-D-galactopyranosyl-(1$\rightarrow$4)-β-D-glucopyranoside] monohydrate: a solvomorphism study

Jieye Lin, Allen G. Oliver and Anthony S. Serianni

Acta Cryst. (2021). C**77**, 668–674

STRUCTURAL CHEMISTRY
ISSN 2053-2296

Methyl β-lactoside [methyl β-D-galactopyranosyl-(1→4)-β-D-glucopyranoside] monohydrate: a solvomorphism study

Jieye Lin,[a] Allen G. Oliver[b] and Anthony S. Serianni[a]*

[a]Department of Chemistry and Biochemistry, University of Notre Dame, Notre Dame, IN 46556-5670, USA, and [b]Molecular Structure Facility, University of Notre Dame, Notre Dame, IN 46556-5670, USA. *Correspondence e-mail: aseriann@nd.edu

Received 19 August 2021
Accepted 11 September 2021

Edited by E. Reinheimer, Rigaku Americas Corporation, USA

Keywords: methyl β-lactoside monohydrate; methyl β-D-galactopyranosyl-(1→4)-β-D-glucopyranoside monohydrate; crystal transformation; solvomorphism; X-ray crystal structure; chemical synthesis.

CCDC reference: 2109224

Supporting information: this article has supporting information at journals.iucr.org/c

Methyl β-lactoside [methyl β-D-galactopyranosyl-(1→4)-β-D-glucopyranoside] monohydrate, $C_{13}H_{24}O_{11}\cdot H_2O$, (I), was obtained *via* spontaneous transformation of methyl β-lactoside methanol solvate, (II), during air-drying. Cremer–Pople puckering parameters indicate that the β-D-Gal*p* (β-D-galactopyranosyl) and β-D-Glc*p* (β-D-glucopyranosyl) rings in (I) adopt slightly distorted $^4C_1$ chair conformations, with the former distorted towards a boat form ($B_{C1,C4}$) and the latter towards a twist-boat form ($^{O5}S_{C2}$). Puckering parameters for (I) and (II) indicate that the conformation of the β-Gal*p* ring is slightly more affected than the β-Glc*p* ring by the solvomorphism. Conformations of the terminal *O*-glycosidic linkages in (I) and (II) are virtually identical, whereas those of the internal *O*-glycosidic linkage show torsion-angle changes of 6° in both C—O bonds. The exocyclic hydroxymethyl group in the β-Gal*p* residue adopts a *gt* conformation (C4′ *anti* to O6′) in both (I) and (II), whereas that in the β-Glc*p* residue adopts a *gg* (*gauche–gauche*) conformation (H5 *anti* to O6) in (II) and a *gt* (*gauche–trans*) conformation (C4 *anti* to O6) in (I). The latter conformational change is critical to the solvomorphism in that it allows water to participate in three hydrogen bonds in (I) as opposed to only two hydrogen bonds in (II), potentially producing a more energetically stable structure for (I) than for (II). Visual inspection of the crystalline lattice of (II) reveals channels in which methanol solvent resides and through which solvent might exchange during solvomorphism. These channels are less apparent in the crystalline lattice of (I).

1. Introduction

Hydrate/solvate crystalline compounds (solvomorphs) and their polymorphs have been reported in the pharmaceutical and materials sciences and are responsible for changes in physical and chemical properties (*e.g.* solubility, melting point, and bioactivity) (Rydz *et al.*, 2018; Barbas *et al.*, 2020). Similar studies of saccharides have been reported in crystals of lactose, cellobiose, and trehalose (Beevers & Hansen, 1971; Nagase *et al.*, 2002; Rencurosi *et al.*, 2002; Listiohadi *et al.*, 2005; Nagase *et al.*, 2008). During solid-state ^{13}C NMR studies of methyl β-D-galactopyranosyl-(1→4)-β-D-glucopyranoside (methyl β-lactoside) methanol solvate, (II) (Stenutz *et al.*, 1999), that was selectively labeled with ^{13}C at C1′ and C3′ of the Gal*p* residue, two sets of paired signals arising from labeled C atoms were observed in spectra when only one pair was expected (Zhang *et al.*, 2019). Upon further scrutiny, this behavior was traced to the propensity of crystals of (II) to transform to methyl β-lactoside monohydrate, (I), upon exposure to the atmosphere. We describe herein the crystal structure of methyl β-D-galactopyranosyl-(1→4)-β-D-glucopyranoside monohydrate, a new crystalline form of methyl β-lactoside that was obtained as a solvomorph of (II) (Scheme 1,

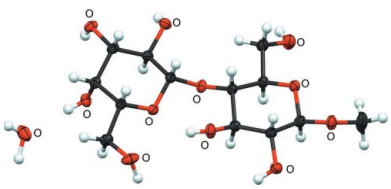

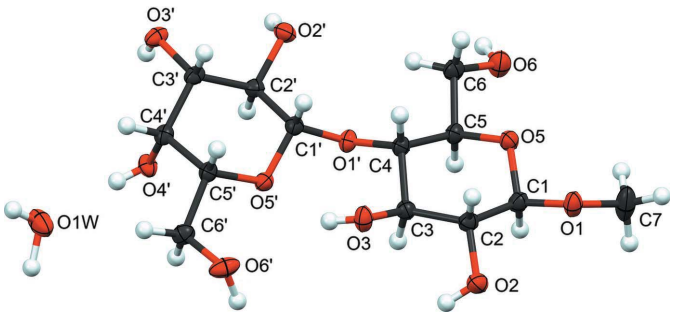

Figure 1
The molecular structure of (I), showing the atom numbering. Displacement ellipsoids are drawn at the 50% probability level and H atoms are shown as small spheres of arbitrary radii.

showing ϕ, ϕ', and ψ', and Fig. 1). In the following discussion, the structures of (I) and (II) are compared to evaluate the effects of solvent replacement on structural parameters and packing structure.

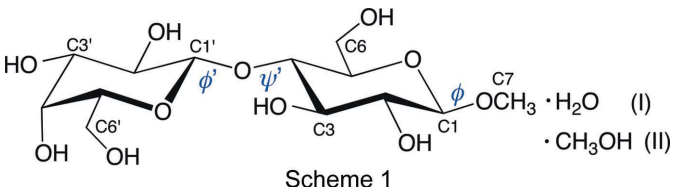

Scheme 1

2. Experimental

2.1. Synthesis and crystallization

2.1.1. Synthesis of methyl β-lactoside, (II′) (Fig. 2). Acetic anhydride (6.67 ml, 70.58 mmol) was added to a solution of (III) (1.51 g, 4.41 mmol) in pyridine (10 ml) and the resulting mixture was stirred at 343 K overnight. The reaction mixture was diluted with CH_2Cl_2 (20 ml) and the solution was poured into ice-cold water (20 ml). The solution was extracted twice with CH_2Cl_2 (2 × 30 ml), and the organic phases were combined and concentrated at 313 K *in vacuo*. Purification by flash chromatography on a silica-gel column (14 × 3.5 cm) (eluent: ethyl acetate/hexanes, 1:1 *v*/*v*) afforded (IV) in 69% yield (2.06 g, 3.04 mmol). ^{1}H and ^{13}C{^{1}H} NMR spectra obtained for (IV) were consistent with those reported previously (Šardzík *et al.*, 2010).

Benzylamine (0.43 ml, 3.95 mmol) was added to a solution of (IV) (2.06 g, 3.04 mmol) in tetrahydrofuran (THF; 21 ml) and the resulting mixture was stirred at 293 K for 2 h. The reaction mixture was concentrated *in vacuo* at 303 K, diluted with ethyl acetate (40 ml), and washed with 0.1 *M* aqueous HCl solution (2 × 20 ml), saturated aqueous $NaHCO_3$ solution (2 × 20 ml), and distilled water (2 × 20 ml). The organic phases were collected and dried *in vacuo* for 2 h to afford crude 2,3,6,2′,3′,4′,6′-hepta-*O*-acetyllactose as a syrup. The crude syrup was dissolved in anhydrous CH_2Cl_2 (20 ml), CCl_3CN (2.43 ml, 2.42 mmol) and DBU (200 µl, 1.34 mmol) were added, and the resulting mixture was stirred at 293 K for 2 h. The reaction mixture was then concentrated at 303 K *in vacuo* and purified by flash chromatography on a silica-gel column (12 × 2.5 cm; eluted with ethyl acetate/hexanes, 2:1 *v*/*v*) to afford (V) in 76% yield in two steps (1.81 g, 2.32 mmol). ^{1}H and ^{13}C{^{1}H} NMR spectra obtained for (V) were consistent with those reported previously (Anraku *et al.*, 2017).

A mixture of (V) (1.81 g, 2.32 mmol), anhydrous methanol (0.47 ml, 11.60 mmol), and freshly activated 5 Å molecular sieves (0.80 g) in anhydrous CH_2Cl_2 (18 ml) was stirred under an N_2 atmosphere at 273 K. TMSOTf (100 µl) was then added and the resulting mixture stirred at 273 K for 2 h. The reaction was quenched with the addition of Et_3N (1 ml), and the mixture was filtered and concentrated *in vacuo*. The residue was purified by flash chromatography on a silica-gel column (12 × 2.5 cm; eluted with ethyl acetate/hexanes, 2:1 *v*/*v*) to afford (VI) in 70% yield (1.06 g, 1.63 mmol). ^{1}H and ^{13}C{^{1}H} NMR spectra obtained for (VI) were consistent with those reported previously (Scheppokat *et al.*, 2003).

Sodium methoxide (25% solution in MeOH, 600 µl) was added to a solution of (VI) (1.06 g, 1.63 mmol) in methanol (15 ml) and the resulting mixture was stirred at 293 K for 2 h. The mixture was neutralized with the batchwise addition of Dowex H^+ cation-exchange resin, filtered to remove the resin, and the filtrate collected and dried *in vacuo*. The residue was dissolved in a minimal volume of distilled water and purified on a column containing Biogel P-2 (110 × 8 cm; eluted with distilled water) to afford (II′) in 80% yield (0.46 g, 1.30 mmol). ^{1}H NMR (600 MHz, ^2H_2O): δ 4.46 (*d*, $J_{H1',H2'}$ = 7.8 Hz, 1H, H-1′), 4.42 (*d*, $J_{H1,H2}$ = 8.0 Hz, 1H, H-1), 4.00 (*dd*, $J_{H6a,H6b}$ = −12.3, $J_{H5,H6a}$ = 2.1 Hz, 1H, H-6*a*), 3.94 (*dd*, *J* = 3.4, 0.5 Hz, 1H, H-4′), 3.82 (*dd*, $J_{H6a,H6b}$ = −12.3, $J_{H5,H6b}$ = 5.1 Hz, H-6*b*), 3.72–

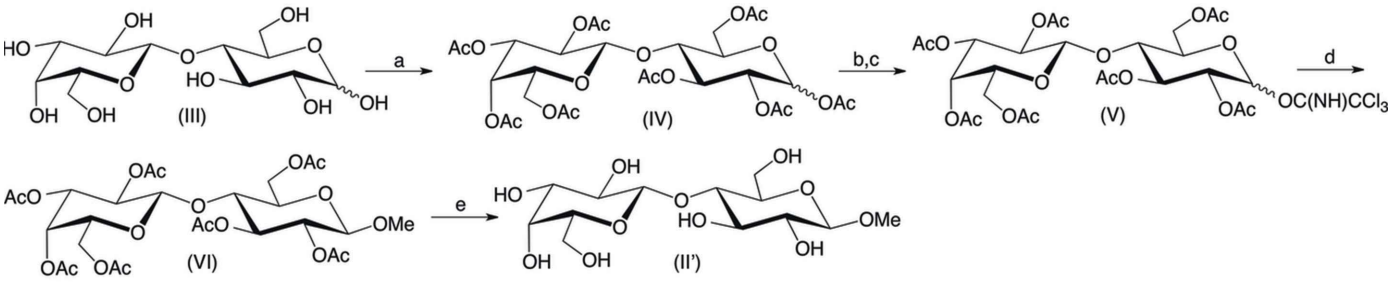

(a) Ac_2O, Py, 80 ºC, 69%; (b) $BnNH_2$, THF; (c) $CNCl_3$, DBU, DCM, 76% for steps (b) + (c); (d) MeOH, TMSOTf, 5Å sieves, DCM, 70%; (e) MeONa, MeOH, 80%.

Figure 2
Synthesis of methyl β-lactoside, (II′).

Table 1
Experimental details.

Crystal data	
Chemical formula	$C_{13}H_{24}O_{11}\cdot H_2O$
M_r	374.34
Crystal system, space group	Monoclinic, $P2_1$
Temperature (K)	120
a, b, c (Å)	4.6250 (1), 24.0147 (7), 7.6617 (2)
β (°)	105.595 (1)
V (Å^3)	819.64 (4)
Z	2
Radiation type	Cu $K\alpha$
μ (mm^{-1})	1.18
Crystal size (mm)	0.18 × 0.17 × 0.05
Data collection	
Diffractometer	Bruker APEXII CCD
Absorption correction	Numerical (*SADABS*; Krause *et al.*, 2015)
T_{min}, T_{max}	0.581, 0.738
No. of measured, independent and observed [$I > 2\sigma(I)$] reflections	14059, 3056, 3031
R_{int}	0.025
(sin $\theta/\lambda)_{max}$ (Å^{-1})	0.612
Refinement	
$R[F^2 > 2\sigma(F^2)]$, $wR(F^2)$, S	0.026, 0.071, 1.04
No. of reflections	3056
No. of parameters	263
No. of restraints	2
H-atom treatment	H atoms treated by a mixture of independent and constrained refinement
$\Delta\rho_{max}$, $\Delta\rho_{min}$ (e Å^{-3})	0.31, −0.16
Absolute structure	Flack x determined using 1459 quotients $[(I^+) - (I^-)]/[(I^+) + (I^-)]$ (Parsons *et al.*, 2013)
Absolute structure parameter	0.05 (4)

Computer programs: *APEX3* (Bruker, 2018), *SAINT* (Bruker, 2018), *SHELXT2014* (Sheldrick, 2015*a*), *SHELXL2018* (Sheldrick, 2015*b*), and *Mercury* (Macrae *et al.*, 2020).

3.80 (*m*, 3H, H-6′*a*, H-6′*b*, H-5′), 3.69–3.64 (*m*, 3H, H-3′, H-3, H-4), 3.61 (*m*, 1H, H-5), 3.59 (*d*, 3H, –OCH$_3$), 3.56 (*dd*, $J_{H2',H3'} = 10.4$, $J_{H1',H2'} = 7.8$ Hz, 1H, H-2′), 3.32 (*dd*, $J_{H1,H2} = 8.0$, $J_{H2,H3} = 9.5$ Hz, 1H, H-2). $^{13}C\{^1H\}$ NMR (150 MHz, ^2H_2O): δ 104.4 (C-1′), 104.3 (C-1), 79.7 (C-4), 76.7 (C-5′), 76.1 (C-5), 75.7 (C-3), 74.1 (C-2), 73.8 (C-3′), 72.3 (C-2′), 69.9 (C-4′), 62.3 (C-6′), 61.4 (C-6), 58.5 (–OCH$_3$). ^1H and $^{13}C\{^1H\}$ NMR spectral data obtained for (II′) were consistent with those reported previously (Hayes *et al.*, 1982; Fernández & Jiménez-Barbero, 1993).

2.1.2. Crystallization of methyl β-lactoside, (II′), to give methanol solvate (II) and monohydrate (I). Compound (II′) was dissolved in a minimal volume of anhydrous methanol. The resulting solution was left at room temperature to allow the solvent to evaporate slowly. Colorless tablet-like crystals of (II) were collected over an approximate 1 week period. Crystals of (II), after exposure to the atmosphere on a laboratory bench for ∼4 d, gave a PXRD pattern that differed from the simulated PXRD pattern of (II), indicating changes in the unit cell (Fig. S2 in the supporting information). The ^1H NMR spectrum of the atmosphere-exposed crystals dissolved in DMSO-d_6 indicated that the methanol was quantitatively replaced by water to give colorless tablet-like crystals of (I) (Fig. S3).

2.2. Refinement

Crystal data, data collection, and structure refinement details are summarized in Table 1. The hydroxy H atoms were located in a difference electron-density map and freely refined in cycles of least-squares refinement, while an equal-distance restraint was applied to the O—H bonds in water. All other H atoms were included in geometrically calculated positions, with C—H = 1.00 (methine), 0.99 (methylene), or 0.98 Å (methyl). C—H hydrogens were refined with displacement parameters tied to that of the atom to which they were bonded [$1.2U_{eq}$(C) for methine and methylene, and $1.5U_{eq}$(C,O) for methyl and hydroxy]. The absolute configuration was determined by comparison with the known chirality of the molecule and by comparison of Friedel pairs of reflections [Flack x parameter = 0.05 (4); Parsons *et al.*, 2013].

3. Results and discussion

Crystals of (II) were obtained from anhydrous methanol in the monoclinic space group $P2_1$, as described previously (Stenutz *et al.*, 1999). Air-drying of these crystals spontaneously transformed them into (I) (monoclinic, $P2_1$), with a dramatic shortening (1.102 Å) in the length of the b axis of the unit cell. This crystal transformation is similar to the formation of crystalline α-lactose monohydrate, whose anhydrous crystalline form is unstable and hygroscopic, and requires one molecule of water to stabilize the crystal lattice (Beevers *et al.*, 1971; Listiohadi *et al.*, 2005).

Cremer–Pople puckering parameters (Cremer & Pople, 1975) indicate that both the β-Gal*p* and β-Glc*p* rings in (I) and (II) adopt distorted $^4C_1$ chair conformations ($q_3 >> q_2$) (Table 2). The chair distortion (encoded in values of θ) is greater in the β-Glc*p* (θ = 10–12°) than in the β-Gal*p* residue (θ = 2–5°) in both (I) and (II), and conversion of the methanol solvate to the monohydrate form results in less distortion in both aldohexopyranosyl rings. The direction of distortion (encoded in values of ϕ) of the β-Glc*p* ring towards a twist-boat form ($^{O5}S_{C2}$) is essentially the same in (I) and (II), whereas the β-Gal*p* ring distorts towards a boat form ($B_{C1,C4}$) in (I) and a twist-boat form ($^{C3}S_{C1}$) in (II). The puckering parameters indicate that the β-Gal*p* ring is slightly more affected than the β-Glc*p* ring by the solvomorphism (slightly larger reduction in θ and a much larger change in ϕ relative to the β-Glc*p* ring), which may explain recent solid-state ^{13}C NMR spectra obtained on selectively ^{13}C-labeled isotopomers of (II) in which two sets of signals were observed for C1′ and C3′ of the β-Gal*p* ring (one set arising from the MeOH solvate and one from the monohydrate), but only one set was observed for C1 and C3 of the β-Glc*p* ring (signals from both solvate forms are presumably degenerate) (Zhang *et al.*, 2019).

Comparisons of corresponding structural parameters in (I) and (II) (Table 3) are complicated by: (*a*) differences in ring conformations, especially for the β-Gal*p* residue (see discussion above and Table 2); (*b*) differences in hydrogen-bond networks in the lattices (Table 4); and (*c*) differences in exocyclic C—O bond torsions (Table 3). For example,

Table 2
Cremer–Pople structural parameters for the βGlc*p* and βGal*p* rings in (I) and (II).

Compound/residue	ϕ (°)	θ (°)	Q (Å)	q_2	q_3
(I)/βGal*p*	70.168	1.912	0.594	0.020	0.594
(I)/βGlc*p*	340.062	9.947	0.569	0.098	0.560
(II)/βGal*p*	28.171	4.675	0.595	0.049	0.593
(II)/βGlc*p*	341.473	11.993	0.558	0.116	0.546

hydrogen bonding involving the exocyclic hydroxy and ring O atoms of the βGal*p* rings of (I) and (II) are very similar, but not for the βGlc*p* rings. In the latter, significantly different hydrogen bonding occurs at O1, O2, and O5. Furthermore, inspection of exocyclic C—O torsion angles involving hydroxy H atoms, which have larger errors than torsion angles involving heavy atoms, reveals differences between (I) and (II), notably for the C2′—C3′—O3′—H, C3′—C4′—O4′—H, and C5′—C6′—O6′—H angles in the βGal*p* residue (Table 3). In general, factors (*a*) and (*c*) are more likely to influence endocyclic C—C and C—O bond lengths, whereas factor (*b*) is more likely to affect exocyclic (hydroxy) C—O bond lengths.

A plot of the C—C and C—O bond lengths in (I) and (II) (Fig. S1 in the supporting information) shows that the C2—C3, C4′—C5′, and C5′—O5′ bonds are significantly longer in (I) than in (II). These changes may be caused mainly by differences in hydrogen bonding at O2 (affecting r_{C2-O2}), and differences in βGal*p* ring conformation (affecting $r_{C4'-C5'}$ and $r_{C5'-O5'}$). The shortest exocyclic C—O bonds in (I) and (II) are C1—O1 and C1′—O1, while the C1—O5 and C1′—O5′ bonds have lengths comparable to all other C—O bonds in (I) and (II). Since O5 and O5′ lone-pair donation to the endocyclic C1—O5 and C1′—O5′ bonds, respectively, in (I) and (II) cannot occur (all residues have the β-configuration), the *endo*-anomeric effect is negligible (Tvaroŝka & Bleha, 1989; Juaristi & Cuevas, 1994). Thus, the *exo*-anomeric effect (Tvaroŝka & Bleha, 1989; Thøgersen *et al.*, 1982) dominates in (I) and (II) wherein both ϕ and ϕ' (Table 3) adopt values that orient C7 and C4 approximately *anti* to C2 and C2′, respectively. These conformations explain the observed C1—O1 and C1′—O1′ bond length truncation, but concomitant C1—O5 and C1′—O5′ bond elongation is not observed. The C1—O1 and C1′—O1′ bond lengths will also be influenced by their equatorial orientations, which generally favor shorter bonds relative to axial orientations in the absence of stereoelectronic effects.

Corresponding exocyclic C1—O1—CH_3 and C1′—O1′—C4 bond angles are essentially the same in (I) and (II), but differ from each other, giving average values of 113.9 ± 0.2 and 116.4 ± 0.2°, respectively (Table 3). The slightly larger C1′—O1′—C4 angle may be caused by the different steric demands of the glycone substituents (small CH_3 *versus* larger aldohexopyranosyl ring). In contrast, the endocyclic C5—O5—C1 and C5′—O5′—C1′ bond angles adopt very similar values in (I) and (II), giving an average value of 112.2 ± 0.2°.

The *O*-glycosidic linkage conformations in (I) and (II) are characterized by two *phi* values (ϕ and ϕ') and a single *psi* value (ψ') (Scheme 1). Torsion angle ϕ, corresponding to the terminal linkage, is virtually unchanged in (I) and (II),

Table 3
Select structural parameters (Å, °) in (I) and (II).

	C—C bond lengths[a]	(I)	(II)
1	C1′—C2′	1.524 (3)	1.527 (3)
2	C2′—C3′	1.528 (3)	1.531 (3)
3	C3′—C4′	1.520 (3)	1.521 (3)
4	C4′—C5′	1.530 (3)	1.521 (3)
5	C5′–C6′	1.515 (3)	1.511 (3)
6	C1—C2	1.522 (3)	1.516 (4)
7	C2—C3	1.528 (3)	1.519 (3)
8	C3—C4	1.530 (3)	1.531 (3)
9	C4—C5	1.524 (3)	1.530 (3)
10	C5—C6	1.512 (3)	1.508 (3)
	C—O bond lengths		
1	C1′—O1′	1.392 (3)	1.387 (3)
2	C1′—O5′	1.429 (2)	1.425 (3)
3	C2′—O2′	1.421 (3)	1.414 (3)
4	C3′—O3′	1.419 (3)	1.422 (3)
5	C4′—O4′	1.423 (3)	1.423 (3)
6	C5′—O5′	1.445 (3)	1.432 (3)
7	C6′—O6′	1.420 (3)	1.426 (3)
8	C1—O1	1.390 (3)	1.384 (3)
9	C1—O5	1.423 (2)	1.413 (3)
10	C2—O2	1.407 (2)	1.418 (3)
11	C3—O3	1.422 (3)	1.421 (3)
12	O1′—C4	1.431 (3)	1.437 (3)
13	C5—O5	1.435 (3)	1.428 (3)
14	C6—O6	1.422 (3)	1.424 (3)
	Internuclear distances		
	$O3_d\cdots O5'$	2.782 (2)	2.764 (2)
	$O3_d\cdots O6'^{ii}$	3.272 (3)	2.935 (3)
	$H_2O\cdots O5_a{}^{i}$	2.890 (2)	–
	$H_2O\cdots O6_a{}^{iv}$	2.811 (3)	–
	$O4'_d\cdots H_2O$	2.686 (3)	–
	$CH_3OH\cdots O6_a$	–	2.727 (3)
	$O4'_d\cdots CH_3OH$	–	2.686 (11)
	Bond angles		
	C5—O5—C1	112.0 (2)	112.0 (2)
	C5′—O5′—C1′	112.3 (2)	112.3 (2)
	C1′—O1′—C4	116.5 (2)	116.2 (2)
	C1—O1—CH_3	114.0 (2)	113.7 (2)
	Torsion angles		
	C1—C2—C3—C4	−46.4 (2)	−44.2 (3)
	C1—O5—C5—C4	66.9 (2)	67.6 (2)
	C1′—C2′—C3′—C4′	−7.1 (2)	−54.8 (2)
	C1′—O5′—C5′—C4′	61.6 (2)	65.0 (2)
	O5—C1—O1—CH_3 (ϕ)	−78.2 (2)	−77.3 (3)
	C2—C1—O1—CH_3 (ϕ)	163.2 (2)	164.2 (2)
	H1—C1—O1—CH_3 (ϕ)	42.2	44.1 (4)
	O5′—C1′—O1′—C4 (ϕ')	−94.0 (2)	−88.4 (2)
	C2′—C1′—O1′—C4 (ϕ')	147.6 (2)	153.8 (2)
	H1′—C1′—O1′—C4 (ϕ')	26.1	31.9 (3)
	C1′—O1′—C4—C3 (ψ')	85.2 (2)	78.4 (2)
	C1′—O1′—C4—C5 (ψ')	−154.5 (2)	−161.3 (2)
	C1′—O1′—C4—H4 (ψ')	−36.0	−43.7 (3)
	O5—C5—C6—O6 (ω)	69.4 (2) (*gt*)	−54.6 (2) (*gg*)
	C4—C5—C6—O6 (ω)	−171.3 (2) (*gt*)	66.4 (3) (*gg*)
	O5′—C5′—C6′—O6′ (ω')	60.8 (2) (*gt*)	57.3 (2) (*gt*)
	C4′—C5′—C6′—O6′ (ω')	−178.4 (2) (*gt*)	177.8 (2) (*gt*)
	C1—C2—O2—H	−125.6	−123.4
	C2—C3—O3—H	−166.6	−159.0
	C5—C6—O6—H	133.0	−123.1
	C1′—C2′—O2′—H	153.5	143.4
	C2′—C3′—C3′—H	68.1	44.9
	C3′—C4′—O4′—H	−142.2	−112.3
	C5′—C6′—O6′—H	−115.3	−132.5

Note: (*a*) C—C and C—O bond-length numbers shown in the left-most column were used to plot the data in Fig. S1 (in the supporting information). Subscript 'a' denotes the acceptor site and subscript 'd' the donor atom in the hydrogen bond. [Symmetry codes: (i) $-x+1, y-\frac{1}{2}, -z+1$; (ii) $x+1, y, z+1$; (iv) $x, y, z+1$.]

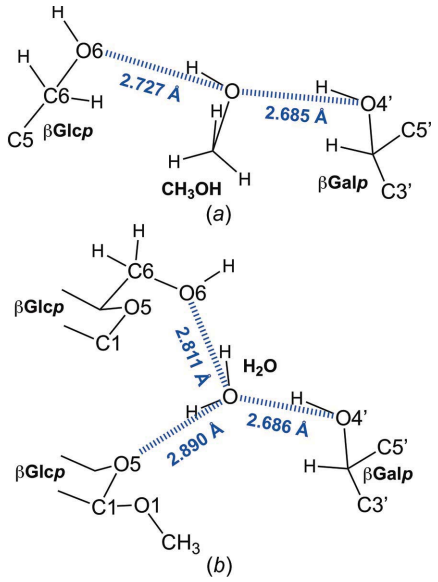

Figure 3
Summary of the hydrogen-bonding interactions involving (*a*) methanol solvent and (*b*) water molecules observed in the crystal structures of (II) and (I), respectively. The *β*Glc*p* and *β*Gal*p* residues are identified and the blue hatched lines denote hydrogen bonds with the associated heavy-atom internuclear distances measured in the crystals (Table 3).

assuming values of 163.2 (2) and 164.2 (2)°, respectively, when the angle is defined by the C2—C1—O1—CH_3 pathway (Table 3). In contrast, the conformation of the internal linkage is affected, albeit minimally, by the solvent. Torsion ϕ' adopts values of 147.6 (2)° in (I) and 153.8 (2)° in (II) when the angle is defined by the C2′—C1′—O1′—C4 pathway, a ∼6° difference (Table 3). Likewise, torsion angle ψ' adopts values of 85.2 (2)° in (I) and 78.4 (2)° in (II) when defined by the C1′—O1′—C4—C3 pathway, a ∼7° difference. The observed values of ϕ and ϕ' are associated with anomeric C—O bond conformations predicted to be the most stable in *β*-anomers based on stereoelectronic considerations (Tvaroŝka & Bleha, 1989; Juaristi & Cuevas, 1994).

The exocyclic hydroxymethyl groups in the *β*Gal*p* residues of (I) and (II) adopt the *gt* (*gauche–trans*) conformation, with minor differences in the O5′—C5′—C6′—O6′ (59.1 ± 2.5°) and C4′—C5′—C6′—O6′ (179.7 ± 2.7°) torsion angles (Table 3). In contrast, the hydroxymethyl group conformation differs significantly in the *β*Glc*p* residues, adopting a *gt* conformation in (I) [respective values of 69.4 (2) and −171.3 (2)°] and a *gg* (*gauche–gauche*) conformation in (II) [respective values of −54.6 (2) and 66.4 (3)°] (Table 3), the two rotamers about ω that are favored in *β*Glc rings in aqueous solution (Bock & Duus, 1994; Rockwell & Grindley, 1998; Thibaudeau *et al.*, 2004). This conformational change plays a key role in the spontaneous conversion of (II) to (I) since the exocyclic hydroxymethyl O atom of the *β*Glc*p* residue participates in saccharide–solvent interactions in both methanol solvate (II) and monohydrate (I). This role is illustrated in Fig. 3 where hydrogen bonding involving solvent in crystals of (I) and (II) is summarized. In (II), the methanol molecule participates in two hydrogen bonds, one to O6 of *β*Glc*p* (acceptor) and one to O4′ of *β*Gal*p* (donor). Two of these hydrogen bonds are maintained in (I), but an additional hydrogen bond is observed between H_2O and atom O5 of *β*Glc*p* (acceptor). In this manner, the full hydrogen-bond-donor capacity of water is achieved, as found for methanol. An inspection of the packing structure of (II) shows that the ring O atoms of the *β*Glc*p* residues are proximal to the methanol molecule but are unable to hydrogen bond to it. The substitution of water at the same binding site apparently results in a small but consequential shift in the location of the solvent binding site and/or possible small shifts in the saccharide matrix, thereby allowing the third hydrogen bond to form. The formation of a third hydrogen bond in (I) may be an important driving force favoring the formation of (I) from (II), although other factors may contribute, including (*a*) differences in the number and strengths of the large ensemble of saccharide–saccharide hydrogen bonds in crystals of (I) and (II), (*b*) the presence of noncovalent sugar stacking interactions in (I) and/or (II), and, importantly, (*c*) global changes in the structure of the crystalline lattice that may favor the conversion of (II) to (I). In the latter regard, visual inspection of the crystal lattice of (II) reveals channels in which the methanol solvent resides and through which solvent might pass during solvomorphism. These channels, whose volumes are partly occupied by the solvent molecule, are narrower in (I) (*i.e.* the crystal lattice is more condensed), leading to the possibility that once (II) converts to (I), solvent exchange may be hindered, although perhaps still feasible, since solvent is less able to penetrate the crystal.

To evaluate the interconvertibility of (I) and (II), an approximate 30 mg sample of crystalline (I) was placed in a

Table 4
Hydrogen-bond geometry (Å, °) of (I) and (II).

Weak hydrogen bond O3—H3O···O6′ was not shown as $D\cdots A > 3.0$ Å.

	D—H···A	D—H	H···A	D···A	D—H···A
(I)	Sugar–solvent interactions				
	O1*W*—H1*WA*···O5^{i}	0.92 (4)	1.97 (4)	2.890 (3)	172 (5)
	O1*W*—H1*WB*···O6^{iv}	0.95 (3)	1.87 (4)	2.811 (3)	176 (4)
	O4′—H4O′···O1*W*	0.77 (3)	1.92 (3)	2.686 (3)	175 (3)
	Sugar–sugar interactions				
	O2—H2O···O2′^{iii}	0.83 (3)	1.98 (3)	2.771 (2)	160 (3)
	O3—H3O···O5′	0.79 (4)	2.10 (4)	2.782 (2)	145 (3)
	O6—H6O···O1^{ii}	0.88 (4)	1.92 (4)	2.795 (2)	169 (3)
	O2′—H2O′···O3^{ii}	0.76 (5)	2.02 (5)	2.763 (2)	167 (5)
	O3′—H3O′···O6′^{ii}	0.71 (4)	2.04 (4)	2.709 (2)	156 (4)
	O6′—H6O′···O3′^{iii}	0.93 (4)	1.72 (4)	2.647 (2)	177 (3)
(II)	Sugar–solvent interactions				
	O4′—H4′O···O11^{i}	0.82 (1)	1.87	2.686 (3)	171
	O11—H11O···O6	0.82 (1)	1.93	2.727 (3)	164
	Sugar–sugar interactions				
	O2—H2O···O2′^{iii}	0.82 (2)	1.96	2.757 (3)	163
	O3—H3O···O5′	0.82 (2)	2.08	2.764 (2)	141
	O6—H6O···O2^{ii}	0.82 (2)	1.94	2.748 (2)	169
	O2′—H2′O···O3^{iv}	0.82 (2)	1.96	2.775 (3)	175
	O3′—H3′O···O6′^{iv}	0.82 (2)	1.96	2.740 (2)	160
	O6′—H6′O···O3′^{iii}	0.820 (7)	1.84	2.662 (2)	175

Symmetry codes for (I): (i) $-x+1, y-\frac{1}{2}, -z+1$; (ii) $x, y, z-1$; (iii) $x+1, y, z+1$; (iv) $-x+2, y-\frac{1}{2}, -z+1$. Symmetry codes for (II): (i) $-x+2, y-\frac{1}{2}, -z+2$; (ii) $x+1, y, z+1$; (iii) $x-1, y, z-1$; (iv) $x, y, z+1$.

20 ml glass vial which was sealed with perforated parafilm to allow gas exchange and placed in a sealed 150 ml glass container containing 1 ml of anhydrous methanol. After incubation for 6 d, the crystals were retrieved and analyzed by PXRD (Fig. S4 in the supporting information). The results showed the presence of crystalline (I) and (II). A Reitveld refinement program (*Profex*; Doebelin & Kleeberg, 2015) was used to process the PXRD data and calculate a composition

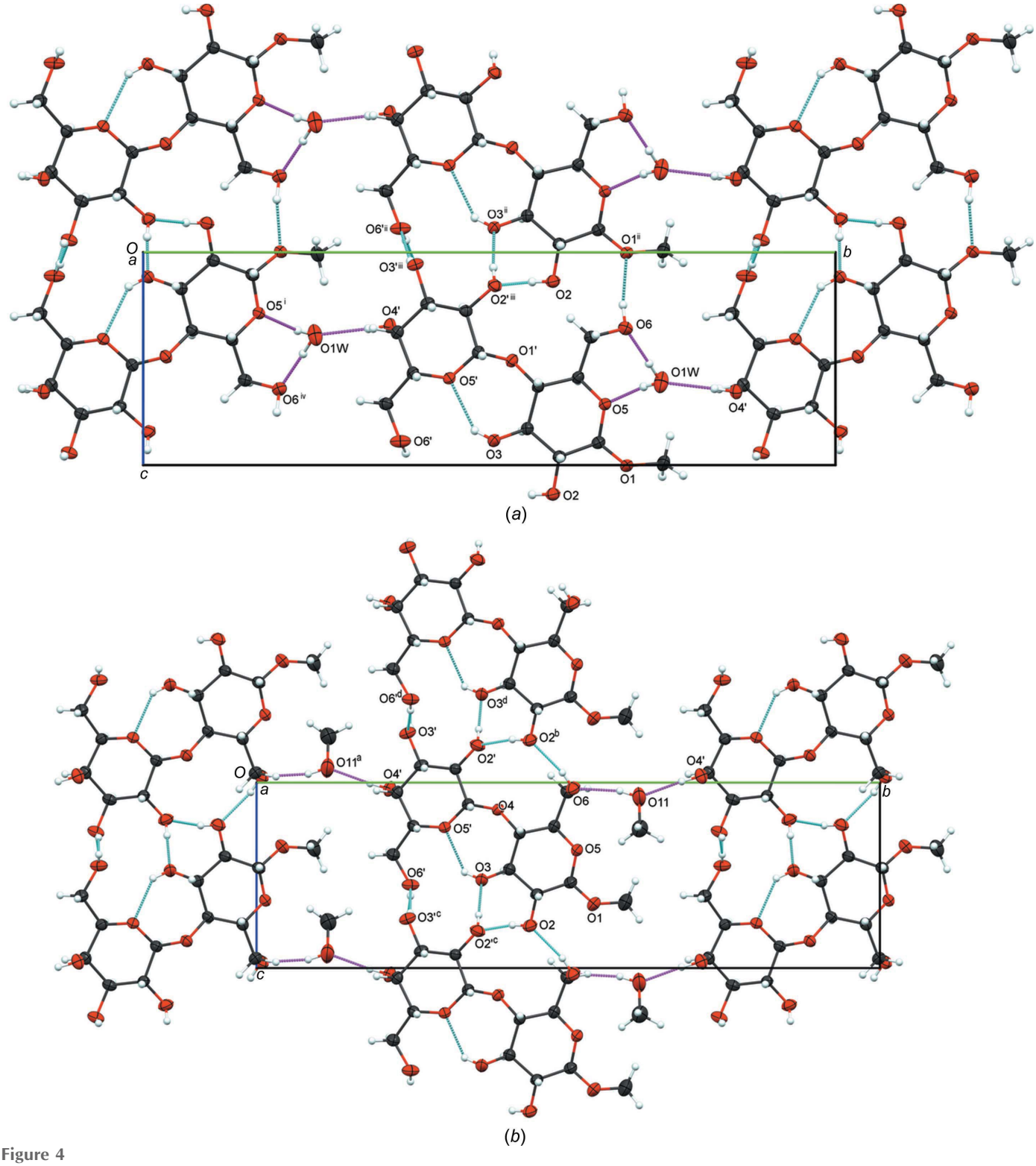

Figure 4
The packing diagrams of (*a*) (I) and (*b*) (II), viewed along the *a* axis. The blue dashed bonds identify sugar–sugar hydrogen bonds and magenta dashed bonds identify sugar–solvent hydrogen bonds. Atoms involved in hydrogen bonding are labeled for clarity. [Symmetry codes: (i) $-x+1, y-\frac{1}{2}, -z+1$; (ii) $x, y, z-1$; (iii) $x+1, y, z+1$; (iv) $-x+2, y-\frac{1}{2}, -z+1$; (a) $-x+2, y-\frac{1}{2}, -z+2$; (b) $x+1, y, z+1$; (c) $x-1, y, z-1$; (d) $x, y, z+1$.]

ratio of the monohydrate and methanol solvate. A (II):(I) ratio of 0.49:0.51 was found, indicating that the conversion of (I) to (II) can occur despite the apparent physical properties of the lattice of (I) that might impede this exchange (Fig. S5 and Table S1 in the supporting information). However, it should be appreciated that the mechanism by which (I) is converted to (II) during the above experiment may not involve only gaseous diffusion of MeOH into crystals of (I) and concomitant displacement of water. The relatively high concentration of MeOH in the gas phase may be sufficient to promote crystal dissolution and recrystallization on a micro scale, which would produce crystals of (II) over time. If the latter mechanism pertains, differences in lattice structures between (I) and (II) would play no role in the solvomorphism. A comparison of the two structures, with solvent removed, reveals a void space of ∼22 Å^3 for (I) and a larger void volume of ∼93 Å^3 in (II) (Fig. S6) (Macrae *et al.*, 2020). The void volume in (II) is connected to form a narrow channel in the lattice parallel to the *a* axis, while in (I) the voids are discrete pockets, perhaps indicating the means of egress and ingress of solvent in the lattice.

Interresidue hydrogen bonding involving atom O3 as a donor and O5′ as an acceptor is observed in both (I) and (II), with comparable internuclear distances [2.782 (2) and 2.764 (2) Å, respectively; Table 3]. The conformation of the exocyclic hydroxymethyl group in (II) (*gg* rotamer) orients O6′ close enough to O3 to produce a second, albeit weaker, hydrogen bond, with an internuclear distance of 2.935 (3) Å. Thus, the O3 atom participates in a bifurcated interresidue hydrogen bond in (II). The conformational change in the exocyclic hydroxymethyl group in (I) to the *gt* rotamer increases the distance between atoms O6′ and O3 to 3.272 (3) Å, such that only a single interresidue hydrogen bond is observed in (I).

In the crystal structure of (I), three sugar–solvent hydrogen bonds and six sugar–sugar hydrogen bonds within the lattice form a dense three-dimensional network in the extended packing (Fig. 4). Sugar–sugar hydrogen-bond interactions in (I) can be separated into three groups: (1) an infinite chain with hydrogen bonds alternating between O6′ and O3′ (along the *a* axis); (2) a four-membered chain starting from O2 to O2′, followed by a hydrogen bond from O2′ to O3 that ends with an intramolecular hydrogen bond from O3 to O5′; and (3) hydrogen bonds between O6 and O1 (along the *c* axis). In contrast, the latter two, in addition to hydrogen bonds involving methanol, in the crystal structure of (II) create a seven-membered chain starting from O4′ and ending at O5′. Sugar–solvent hydrogen bonds in (I) and (II) enable the translation along the *b* axis, with one additional O1*W*···O5 contact observed in (I) because water serves as a donor in two hydrogen bonds and a mono-acceptor in one hydrogen bond. Sugar–sugar hydrogen bonds constrain the general crystal structure and create a channel-like gap between two layers of molecules in the unit cell, which presumably permits the egress of methanol from crystals of (II) and the ingress of water to form (I), the latter containing more solvent hydrogen bonds between two antiparallel layers of molecules. The details of the hydrogen bonds and symmetry codes are summarized in Table 4.

Funding information

Funding for this research was provided by: National Science Foundation, Office of the Director (grant Nos. CHE 1707660 and CHE 2002625 to Anthony S. Serianni); Omicron Biochemicals (award to Jieye Lin and Anthony S. Serianni).

References

Anraku, K., Sato, S., Jacob, N. T., Eubanks, L. M., Ellis, B. A. & Janda, K. D. (2017). *Org. Biomol. Chem.* **15**, 2979–2992.
Barbas, R., Kumar, V., Vallcorba, O., Prohens, R. & Frontera, A. (2020). *Crystals*, **10**, 1126.
Beevers, C. A. & Hansen, H. N. (1971). *Acta Cryst.* B**27**, 1323–1325.
Bock, K. & Duus, J. O. (1994). *J. Carbohydr. Chem.* **13**, 513–543.
Bruker (2018). *APEX3* and *SAINT*. Bruker AXS Inc., Madison, Wisconsin, USA.
Cremer, D. & Pople, J. A. (1975). *J. Am. Chem. Soc.* **97**, 1354–1358.
Doebelin, N. & Kleeberg, R. (2015). *J. Appl. Cryst.* **48**, 1573–1580.
Fernández, P. & Jiménez-Barbero, J. (1993). *Carbohydr. Res.* **248**, 15–36.
Hayes, M. L., Serianni, A. S. & Barker, R. (1982). *Carbohydr. Res.* **100**, 87–101.
Juaristi, E. & Cuevas, G. (1994). In *The Anomeric Effect*. Boca Raton: CRC Press.
Krause, L., Herbst-Irmer, R., Sheldrick, G. M. & Stalke, D. (2015). *J. Appl. Cryst.* **48**, 3–10.
Listiohadi, Y. D., Hourigan, J. A., Sleigh, R. W. & Steele, R. J. (2005). *Aust. J. Dairy Technol.* **60**, 33–52.
Macrae, C. F., Sovago, I., Cottrell, S. J., Galek, P. T. A., McCabe, P., Pidcock, E., Platings, M., Shields, G. P., Stevens, J. S., Towler, M. & Wood, P. A. (2020). *J. Appl. Cryst.* **53**, 226–235.
Nagase, H., Endo, T., Ueda, H. & Nakagaki, M. (2002). *Carbohydr. Res.* **337**, 167–173.
Nagase, H., Ogawa, N., Endo, T., Shiro, M., Ueda, H. & Sakurai, M. (2008). *J. Phys. Chem. B*, **112**, 9105–9111.
Parsons, S., Flack, H. D. & Wagner, T. (2013). *Acta Cryst.* B**69**, 249–259.
Rencurosi, A., Röhrling, J., Pauli, J., Potthast, A., Jäger, C., Pérez, S., Kosma, P. & Imberty, A. (2002). *Angew. Chem. Int. Ed.* **41**, 4277–4281.
Rockwell, G. D. & Grindley, T. B. (1998). *J. Am. Chem. Soc.* **120**, 10953–10963.
Rydz, A., Gryl, M. & Stadnicka, K. M. (2018). *Acta Cryst.* C**74**, 1586–1594.
Šardzík, R., Noble, G. T., Weissenborn, M. J., Martin, A., Webb, S. J. & Flitsch, S. L. (2010). *Beilstein J. Org. Chem.* **6**, 699–703.
Scheppokat, A. M., Bretting, H. & Thiem, J. (2003). *Carbohydr. Res.* **338**, 2083–2090.
Sheldrick, G. M. (2015*a*). *Acta Cryst.* A**71**, 3–8.
Sheldrick, G. M. (2015*b*). *Acta Cryst.* C**71**, 3–8.
Stenutz, R., Shang, M. & Serianni, A. S. (1999). *Acta Cryst.* C**55**, 1719–1721.
Thibaudeau, C., Stenutz, R., Hertz, B., Klepach, T., Zhao, S., Wu, Q., Carmichael, I. & Serianni, A. S. (2004). *J. Am. Chem. Soc.* **126**, 15668–15685.
Thøgersen, H., Lemieux, R. U., Bock, K. & Meyer, B. (1982). *Can. J. Chem.* **60**, 44–57.
Tvaroška, I. & Bleha, T. (1989). *Adv. Carbohydr. Chem. Biochem.* **47**, 45–123.
Zhang, W., Yoon, M.-K., Meredith, R. J., Zajicek, J., Oliver, A. G., Hadad, M., Frey, M. H., Carmichael, I. & Serianni, A. S. (2019). *Phys. Chem. Chem. Phys.* **21**, 23576–23588.

supporting information

Acta Cryst. (2021). C**77**, 668-674 [https://doi.org/10.1107/S2053229621009499]

Methyl β-lactoside [methyl β-D-galactopyranosyl-(1→4)-β-D-glucopyranoside] monohydrate: a solvomorphism study

Jieye Lin, Allen G. Oliver and Anthony S. Serianni

Computing details

Data collection: *APEX3* (Bruker, 2018); cell refinement: *SAINT* (Bruker, 2018); data reduction: *SAINT* (Bruker, 2018); program(s) used to solve structure: SHELXT2014 (Sheldrick, 2015a); program(s) used to refine structure: *SHELXL2018* (Sheldrick, 2015b); molecular graphics: *Mercury* (Macrae *et al.*, 2020); software used to prepare material for publication: *SHELXL2018* (Sheldrick, 2015b).

Methyl β-lactoside monohydrate

Crystal data

$C_{13}H_{24}O_{11}·H_2O$
M_r = 374.34
Monoclinic, $P2_1$
a = 4.6250 (1) Å
b = 24.0147 (7) Å
c = 7.6617 (2) Å
β = 105.595 (1)°
V = 819.64 (4) Å^3
Z = 2
$F(000)$ = 400
D_x = 1.517 Mg m^{-3}
Cu $K\alpha$ radiation, λ = 1.54178 Å
Cell parameters from 9961 reflections
θ = 3.7–70.6°
μ = 1.18 mm^{-1}
T = 120 K
Tablet, colourless
0.18 × 0.17 × 0.05 mm

Data collection

Bruker APEXII CCD diffractometer
Radiation source: Ius micro-focus
Detector resolution: 7.41 pixels mm^{-1}
φ and ω scans
Absorption correction: numerical (SADABS; Krause *et al.*, 2015)
T_{min} = 0.581, T_{max} = 0.738
14059 measured reflections
3056 independent reflections
3031 reflections with $I > 2\sigma(I)$
R_{int} = 0.025
θ_{max} = 70.6°, θ_{min} = 3.7°
h = −5→5
k = −29→29
l = −9→9

Refinement

Refinement on F^2
Least-squares matrix: full
$R[F^2 > 2\sigma(F^2)]$ = 0.026
$wR(F^2)$ = 0.071
S = 1.04
3056 reflections
263 parameters
2 restraints
Primary atom site location: dual
Secondary atom site location: difference Fourier map
Hydrogen site location: mixed
H atoms treated by a mixture of independent and constrained refinement
$w = 1/[\sigma^2(F_o^2) + (0.045P)^2 + 0.1553P]$ where $P = (F_o^2 + 2F_c^2)/3$
$(\Delta/\sigma)_{max} < 0.001$
$\Delta\rho_{max}$ = 0.31 e Å^{-3}
$\Delta\rho_{min}$ = −0.16 e Å^{-3}

Absolute structure: Flack *x* determined using 1459 quotients [(I+)-(I-)]/[(I+)+(I-)] (Parsons *et al.*, 2013)
Absolute structure parameter: 0.05 (4)

Special details

Geometry. All esds (except the esd in the dihedral angle between two l.s. planes) are estimated using the full covariance matrix. The cell esds are taken into account individually in the estimation of esds in distances, angles and torsion angles; correlations between esds in cell parameters are only used when they are defined by crystal symmetry. An approximate (isotropic) treatment of cell esds is used for estimating esds involving l.s. planes.

Fractional atomic coordinates and isotropic or equivalent isotropic displacement parameters (Å²)

	x	*y*	*z*	U_{iso}*/U_{eq}
O1	0.6945 (4)	0.69849 (7)	1.0028 (2)	0.0275 (4)
O2	0.8779 (4)	0.59193 (7)	1.1369 (2)	0.0273 (3)
H2O	0.965 (7)	0.5620 (14)	1.139 (4)	0.028 (7)*
O3	0.5847 (4)	0.50682 (7)	0.8846 (2)	0.0267 (3)
H3O	0.621 (7)	0.4792 (15)	0.838 (4)	0.030 (8)*
O5	0.5942 (4)	0.66710 (6)	0.7138 (2)	0.0220 (3)
O6	0.6390 (4)	0.69673 (7)	0.3572 (2)	0.0326 (4)
H6O	0.669 (8)	0.6929 (14)	0.249 (5)	0.042 (9)*
O1′	0.6438 (3)	0.53275 (6)	0.5092 (2)	0.0213 (3)
O2′	0.2953 (4)	0.50780 (7)	0.1565 (2)	0.0242 (3)
H2O′	0.350 (10)	0.5057 (19)	0.072 (6)	0.058 (12)*
O3′	0.2417 (4)	0.39315 (7)	0.0577 (2)	0.0237 (3)
H3O′	0.382 (10)	0.3860 (17)	0.042 (5)	0.046 (11)*
O4′	0.7291 (3)	0.35632 (7)	0.3451 (2)	0.0216 (3)
H4O′	0.764 (6)	0.3249 (13)	0.359 (3)	0.013 (6)*
O5′	0.6327 (3)	0.44224 (6)	0.5922 (2)	0.0205 (3)
O6′	0.6741 (4)	0.37161 (8)	0.8886 (2)	0.0309 (4)
H6O′	0.873 (8)	0.3796 (15)	0.944 (5)	0.040 (8)*
C1	0.7704 (5)	0.65762 (9)	0.8945 (3)	0.0224 (4)
H1	0.989103	0.659580	0.901284	0.027*
C2	0.6930 (5)	0.60125 (9)	0.9609 (3)	0.0212 (4)
H2	0.480366	0.602811	0.967917	0.025*
C3	0.7160 (5)	0.55488 (9)	0.8288 (3)	0.0207 (4)
H3	0.932836	0.547190	0.840480	0.025*
C4	0.5624 (5)	0.57059 (9)	0.6322 (3)	0.0193 (4)
H4	0.339676	0.570235	0.612076	0.023*
C5	0.6628 (5)	0.62815 (9)	0.5886 (3)	0.0207 (4)
H5	0.884366	0.627842	0.603719	0.025*
C6	0.5041 (5)	0.64700 (9)	0.3986 (3)	0.0241 (4)
H6A	0.517498	0.617525	0.310737	0.029*
H6B	0.289288	0.653766	0.389090	0.029*
C7	0.8300 (9)	0.75158 (11)	0.9912 (4)	0.0445 (7)
HA	0.804741	0.761126	0.863563	0.067*
HC	1.044419	0.749864	1.053992	0.067*
HB	0.733355	0.780040	1.047915	0.067*

C1′	0.4761 (5)	0.48398 (9)	0.4699 (3)	0.0190 (4)
H1′	0.270949	0.489827	0.486252	0.023*
C2′	0.4547 (5)	0.46614 (9)	0.2760 (3)	0.0191 (4)
H2′	0.660667	0.461738	0.259442	0.023*
C3′	0.2871 (4)	0.41071 (9)	0.2399 (3)	0.0192 (4)
H3′	0.084205	0.416873	0.259437	0.023*
C4′	0.4446 (5)	0.36713 (8)	0.3764 (3)	0.0194 (4)
H4′	0.322879	0.332145	0.358122	0.023*
C5′	0.4756 (5)	0.38959 (9)	0.5674 (3)	0.0194 (4)
H5′	0.271275	0.394969	0.585597	0.023*
C6′	0.6551 (5)	0.35079 (10)	0.7124 (3)	0.0234 (4)
H6B′	0.558661	0.313657	0.698274	0.028*
H6A′	0.859855	0.346437	0.697257	0.028*
O1W	0.8826 (4)	0.24832 (8)	0.3889 (3)	0.0390 (4)
H1WA	0.738 (9)	0.2209 (19)	0.366 (7)	0.078 (14)*
H1WB	1.050 (8)	0.2317 (16)	0.471 (5)	0.054 (11)*

Atomic displacement parameters (Å²)

	U^{11}	U^{22}	U^{33}	U^{12}	U^{13}	U^{23}
O1	0.0444 (10)	0.0198 (8)	0.0198 (8)	−0.0016 (7)	0.0108 (7)	−0.0025 (6)
O2	0.0329 (8)	0.0269 (8)	0.0197 (7)	0.0076 (7)	0.0026 (6)	−0.0022 (6)
O3	0.0421 (9)	0.0189 (7)	0.0216 (7)	−0.0016 (7)	0.0130 (7)	−0.0021 (6)
O5	0.0288 (8)	0.0198 (7)	0.0172 (7)	0.0032 (6)	0.0057 (6)	−0.0007 (6)
O6	0.0498 (11)	0.0259 (9)	0.0227 (8)	−0.0039 (8)	0.0107 (8)	0.0009 (7)
O1′	0.0233 (7)	0.0201 (7)	0.0216 (7)	−0.0016 (6)	0.0084 (6)	−0.0038 (6)
O2′	0.0267 (8)	0.0250 (7)	0.0202 (7)	0.0069 (6)	0.0053 (6)	0.0029 (6)
O3′	0.0204 (8)	0.0322 (8)	0.0180 (7)	−0.0005 (6)	0.0044 (6)	−0.0056 (6)
O4′	0.0205 (7)	0.0195 (8)	0.0272 (8)	0.0016 (6)	0.0104 (6)	−0.0009 (6)
O5′	0.0218 (7)	0.0196 (7)	0.0184 (7)	−0.0022 (5)	0.0024 (6)	−0.0008 (5)
O6′	0.0220 (8)	0.0529 (11)	0.0177 (7)	−0.0008 (7)	0.0051 (6)	−0.0018 (7)
C1	0.0252 (10)	0.0226 (10)	0.0187 (10)	−0.0012 (8)	0.0046 (8)	−0.0023 (8)
C2	0.0216 (10)	0.0229 (11)	0.0186 (10)	0.0007 (8)	0.0049 (8)	−0.0013 (8)
C3	0.0227 (10)	0.0195 (10)	0.0198 (10)	0.0008 (7)	0.0055 (8)	0.0001 (7)
C4	0.0213 (10)	0.0200 (9)	0.0171 (10)	0.0007 (8)	0.0059 (8)	−0.0023 (8)
C5	0.0233 (10)	0.0202 (10)	0.0190 (10)	0.0011 (8)	0.0062 (8)	−0.0029 (8)
C6	0.0295 (11)	0.0234 (11)	0.0190 (10)	0.0004 (8)	0.0059 (8)	−0.0011 (8)
C7	0.083 (2)	0.0225 (12)	0.0317 (13)	−0.0111 (13)	0.0212 (14)	−0.0059 (10)
C1′	0.0189 (9)	0.0184 (9)	0.0197 (10)	−0.0005 (8)	0.0051 (8)	−0.0017 (7)
C2′	0.0174 (9)	0.0211 (9)	0.0183 (9)	0.0012 (8)	0.0037 (7)	0.0005 (8)
C3′	0.0152 (9)	0.0245 (10)	0.0182 (10)	−0.0014 (7)	0.0050 (8)	−0.0032 (8)
C4′	0.0169 (9)	0.0204 (10)	0.0222 (10)	−0.0023 (7)	0.0074 (8)	−0.0024 (8)
C5′	0.0196 (9)	0.0195 (9)	0.0200 (9)	−0.0027 (7)	0.0068 (8)	−0.0013 (8)
C6′	0.0246 (10)	0.0263 (10)	0.0195 (9)	−0.0019 (8)	0.0062 (8)	0.0012 (8)
O1W	0.0337 (9)	0.0249 (8)	0.0568 (12)	0.0012 (7)	0.0094 (9)	0.0071 (8)

Geometric parameters (Å, º)

O1—C1	1.390 (3)	C3—C4	1.530 (3)
O1—C7	1.434 (3)	C3—H3	1.0000
O2—C2	1.407 (3)	C4—C5	1.524 (3)
O2—H2O	0.82 (3)	C4—H4	1.0000
O3—C3	1.422 (3)	C5—C6	1.512 (3)
O3—H3O	0.79 (4)	C5—H5	1.0000
O5—C1	1.423 (3)	C6—H6A	0.9900
O5—C5	1.435 (2)	C6—H6B	0.9900
O6—C6	1.422 (3)	C7—HA	0.9800
O6—H6O	0.88 (4)	C7—HC	0.9800
O1′—C1′	1.392 (3)	C7—HB	0.9800
O1′—C4	1.430 (2)	C1′—C2′	1.523 (3)
O2′—C2′	1.421 (3)	C1′—H1′	1.0000
O2′—H2O′	0.76 (5)	C2′—C3′	1.528 (3)
O3′—C3′	1.419 (3)	C2′—H2′	1.0000
O3′—H3O′	0.71 (4)	C3′—C4′	1.520 (3)
O4′—C4′	1.424 (3)	C3′—H3′	1.0000
O4′—H4O′	0.77 (3)	C4′—C5′	1.530 (3)
O5′—C1′	1.429 (3)	C4′—H4′	1.0000
O5′—C5′	1.445 (3)	C5′—C6′	1.515 (3)
O6′—C6′	1.420 (3)	C5′—H5′	1.0000
O6′—H6O′	0.93 (4)	C6′—H6B′	0.9900
C1—C2	1.522 (3)	C6′—H6A′	0.9900
C1—H1	1.0000	O1W—H1WA	0.92 (4)
C2—C3	1.527 (3)	O1W—H1WB	0.95 (3)
C2—H2	1.0000		

C1—O1—C7	113.95 (19)	C5—C6—H6B	109.7
C2—O2—H2O	109 (2)	H6A—C6—H6B	108.2
C3—O3—H3O	113 (2)	O1—C7—HA	109.5
C1—O5—C5	111.99 (16)	O1—C7—HC	109.5
C6—O6—H6O	108 (2)	HA—C7—HC	109.5
C1′—O1′—C4	116.57 (16)	O1—C7—HB	109.5
C2′—O2′—H2O′	106 (3)	HA—C7—HB	109.5
C3′—O3′—H3O′	110 (3)	HC—C7—HB	109.5
C4′—O4′—H4O′	108.7 (19)	O1′—C1′—O5′	107.07 (16)
C1′—O5′—C5′	112.29 (15)	O1′—C1′—C2′	109.53 (16)
C6′—O6′—H6O′	108 (2)	O5′—C1′—C2′	109.31 (16)
O1—C1—O5	107.31 (17)	O1′—C1′—H1′	110.3
O1—C1—C2	107.97 (17)	O5′—C1′—H1′	110.3
O5—C1—C2	110.05 (17)	C2′—C1′—H1′	110.3
O1—C1—H1	110.5	O2′—C2′—C1′	108.48 (16)
O5—C1—H1	110.5	O2′—C2′—C3′	110.28 (16)
C2—C1—H1	110.5	C1′—C2′—C3′	108.58 (16)
O2—C2—C1	108.96 (18)	O2′—C2′—H2′	109.8
O2—C2—C3	112.73 (18)	C1′—C2′—H2′	109.8

C1—C2—C3	111.25 (18)	C3′—C2′—H2′	109.8
O2—C2—H2	107.9	O3′—C3′—C4′	112.89 (18)
C1—C2—H2	107.9	O3′—C3′—C2′	111.77 (17)
C3—C2—H2	107.9	C4′—C3′—C2′	110.44 (16)
O3—C3—C2	106.35 (17)	O3′—C3′—H3′	107.1
O3—C3—C4	111.91 (18)	C4′—C3′—H3′	107.1
C2—C3—C4	112.09 (17)	C2′—C3′—H3′	107.1
O3—C3—H3	108.8	O4′—C4′—C3′	107.68 (17)
C2—C3—H3	108.8	O4′—C4′—C5′	111.86 (17)
C4—C3—H3	108.8	C3′—C4′—C5′	108.64 (17)
O1′—C4—C5	106.40 (16)	O4′—C4′—H4′	109.5
O1′—C4—C3	110.95 (17)	C3′—C4′—H4′	109.5
C5—C4—C3	110.59 (17)	C5′—C4′—H4′	109.5
O1′—C4—H4	109.6	O5′—C5′—C6′	106.55 (16)
C5—C4—H4	109.6	O5′—C5′—C4′	110.39 (16)
C3—C4—H4	109.6	C6′—C5′—C4′	112.11 (17)
O5—C5—C6	108.13 (17)	O5′—C5′—H5′	109.2
O5—C5—C4	108.03 (16)	C6′—C5′—H5′	109.2
C6—C5—C4	112.65 (17)	C4′—C5′—H5′	109.2
O5—C5—H5	109.3	O6′—C6′—C5′	111.23 (18)
C6—C5—H5	109.3	O6′—C6′—H6B′	109.4
C4—C5—H5	109.3	C5′—C6′—H6B′	109.4
O6—C6—C5	109.72 (18)	O6′—C6′—H6A′	109.4
O6—C6—H6A	109.7	C5′—C6′—H6A′	109.4
C5—C6—H6A	109.7	H6B′—C6′—H6A′	108.0
O6—C6—H6B	109.7	H1WA—O1W—H1WB	104 (4)

C7—O1—C1—O5	−78.2 (2)	C4—C5—C6—O6	−171.25 (17)
C7—O1—C1—C2	163.2 (2)	C4—O1′—C1′—O5′	−93.96 (19)
C5—O5—C1—O1	177.92 (16)	C4—O1′—C1′—C2′	147.62 (17)
C5—O5—C1—C2	−64.8 (2)	C5′—O5′—C1′—O1′	178.56 (15)
O1—C1—C2—O2	−65.4 (2)	C5′—O5′—C1′—C2′	−62.9 (2)
O5—C1—C2—O2	177.76 (18)	O1′—C1′—C2′—O2′	−63.7 (2)
O1—C1—C2—C3	169.71 (17)	O5′—C1′—C2′—O2′	179.31 (15)
O5—C1—C2—C3	52.9 (2)	O1′—C1′—C2′—C3′	176.47 (16)
O2—C2—C3—O3	68.3 (2)	O5′—C1′—C2′—C3′	59.5 (2)
C1—C2—C3—O3	−168.95 (17)	O2′—C2′—C3′—O3′	57.6 (2)
O2—C2—C3—C4	−169.09 (18)	C1′—C2′—C3′—O3′	176.29 (16)
C1—C2—C3—C4	−46.3 (2)	O2′—C2′—C3′—C4′	−175.87 (16)
C1′—O1′—C4—C5	−154.47 (17)	C1′—C2′—C3′—C4′	−57.1 (2)
C1′—O1′—C4—C3	85.2 (2)	O3′—C3′—C4′—O4′	60.0 (2)
O3—C3—C4—O1′	−73.8 (2)	C2′—C3′—C4′—O4′	−66.0 (2)
C2—C3—C4—O1′	166.84 (17)	O3′—C3′—C4′—C5′	−178.70 (16)
O3—C3—C4—C5	168.41 (16)	C2′—C3′—C4′—C5′	55.4 (2)
C2—C3—C4—C5	49.0 (2)	C1′—O5′—C5′—C6′	−176.46 (16)
C1—O5—C5—C6	−170.91 (17)	C1′—O5′—C5′—C4′	61.6 (2)
C1—O5—C5—C4	66.9 (2)	O4′—C4′—C5′—O5′	62.4 (2)
O1′—C4—C5—O5	−178.01 (15)	C3′—C4′—C5′—O5′	−56.3 (2)

C3—C4—C5—O5	−57.4 (2)	O4′—C4′—C5′—C6′	−56.2 (2)
O1′—C4—C5—C6	62.6 (2)	C3′—C4′—C5′—C6′	−174.95 (17)
C3—C4—C5—C6	−176.81 (18)	O5′—C5′—C6′—O6′	60.8 (2)
O5—C5—C6—O6	69.4 (2)	C4′—C5′—C6′—O6′	−178.35 (17)

Hydrogen-bond geometry (Å, º)

D—H···*A*	*D*—H	H···*A*	*D*···*A*	*D*—H···*A*
O2′—H2*O*′···O3^{i}	0.76 (5)	2.02 (5)	2.763 (2)	167 (5)
O2—H2*O*···O2′^{ii}	0.82 (3)	1.98 (3)	2.770 (2)	160 (3)
O3′—H3*O*′···O6′^{i}	0.71 (4)	2.04 (4)	2.709 (2)	156 (4)
O3—H3*O*···O5′	0.79 (4)	2.10 (4)	2.782 (2)	145 (3)
O3—H3*O*···O6′	0.79 (4)	2.61 (4)	3.272 (3)	142 (3)
O4′—H4*O*′···O1*W*	0.77 (3)	1.92 (3)	2.686 (3)	175 (3)
O6′—H6*O*′···O3′^{ii}	0.93 (4)	1.72 (4)	2.647 (2)	177 (3)
O6—H6*O*···O1^{i}	0.88 (4)	1.92 (4)	2.795 (2)	169 (3)
O1*W*—H1*WA*···O5^{iii}	0.92 (4)	1.97 (4)	2.890 (2)	172 (5)
O1*W*—H1*WB*···O6^{iv}	0.95 (3)	1.87 (3)	2.811 (3)	176 (4)

Symmetry codes: (i) *x*, *y*, *z*−1; (ii) *x*+1, *y*, *z*+1; (iii) −*x*+1, *y*−1/2, −*z*+1; (iv) −*x*+2, *y*−1/2, −*z*+1.